Published in final edited form as:
Nature. 2015 January 22; 517(7535): 513–516. doi:10.1038/nature13901.

Reductive dehalogenase structure suggests a mechanism for B12-dependent dehalogenation

Karl AP Payne[#1], **Carolina P Quezada**[#1], **Karl Fisher**[1], **Mark S Dunstan**[1], **Fraser A Collins**[1], **Hanno Sjuts**[1,‡], **Colin Levy**[1], **Sam Hay**[1], **Stephen EJ Rigby**[1], and **David Leys**[1,*]

[1]Manchester Institute for Biotechnology, University of Manchester, Princess Street 131 M1 7DN Manchester, UK

[#] These authors contributed equally to this work.

Abstract

Organohalide chemistry underpins many industrial and agricultural processes, and a large proportion of environmental pollutants are organohalides1. Nevertheless, organohalide chemistry is not exclusively of anthropogenic origin, with natural abiotic and biological processes contributing to the global halide cycle2–3. Reductive dehalogenases are responsible for biological dehalogenation in organohalide respiring bacteria4–5, with substrates including the notorious polychlorinated biphenyls (PCBs) or dioxins6–7. These proteins form a distinct subfamily of cobalamin (B12) dependent enzymes that are usually membrane-associated and oxygen-sensitive, hindering detailed studies8–12. We report the characterisation of a soluble, oxygen-tolerant reductive dehalogenase and, by combining structure determination with EPR spectroscopy and simulation, show that a direct interaction between the cobalamin cobalt and the substrate halogen underpins catalysis. In contrast to the carbon-Co bond chemistry catalyzed by the other cobalamin-dependent subfamilies13 we propose that reductive dehalogenases achieve reduction of the organohalide substrate via halogen-Co bond formation. This presents a new paradigm in both organohalide and cobalamin (bio)chemistry that will guide future exploitation of these enzymes in bioremediation or biocatalysis.

Cobalamin consists of a cobalt ion coordinated by a tetrapyrrole derived macrocycle and readily forms a weak organometallic C-Co(III) bond14. This bond can be homolytically or heterolytically cleaved and the B12-dependent enzymes can be classified according to the

[*]Correspondence and requests for materials should be addressed to D.L. (david.leys@manchester.ac.uk).
[‡]current address: Institute of Biochemistry, Goethe Universität Frankfurt, Max-von-Laue-Straße 9, 60438 Frankfurt, Germany

Author Contributions K.P., M.D., K.F., H.S. were involved in *rdhA* heterologous production screening. K.P. obtained heterologous expression of active $RdhA_{NP}$ in *B. megaterium*. C.Q. crystallised and solved the $RdhA_{NP}$ structure with assistance from D.L. and C.L.; C.Q., K.P., M.D. and K.F. performed kinetic studies; K.P. and F.C. prepared and analyzed $RdhA_{NP}$ variants. K.F. and S.R. performed and analyzed EPR experiments. S.H. performed docking and DFT calculations. All authors discussed the results and participated in writing the manuscript. D.L. initiated and directed this research.

Author information Coordinates and structure factors have been deposited in the Protein Data Bank under accession number 4RAS. Reprints and permission information is available at www.nature.com/reprints. Readers are welcome to comments on the online version of the paper.

The authors declare no competing financial interest.

Europe PMC Funders Author Manuscripts

type of reaction catalyzed13: (*i*) the 5'-deoxyadenosyl cobalamin (AdoCbl) dependent isomerases that use AdoCbl as a reusable radical via homolytic cleavage of the Co-C bond; (*ii*) the methylcobalamin-dependent methyltransferases that catalyse a heterolytic C-Co(III) cleavage, cycling between cob(I)alamin and methylcob(III)alamin redox states; (*iii*) the reductive dehalogenases. Little is known about the role, if any, of C-Co chemistry in biological reductive dehalogenation.

Following the screening of a range of reductive dehalogenase genes (*rdhA*) for soluble heterologous expression (including recently uncovered catabolic *rdhA* family members15), active protein could be obtained when expressing a reductive dehalogenase homolog from *Nitratireductor pacificus* pht-3B (*rdhA*$_{NP}$) in *Bacillus megaterium*. Heterologous expression in *E. coli* did yield soluble RdhA$_{NP}$, but the enzyme lacked cobalamin. In contrast to the majority of *rdhA* homologs, *rdhA*$_{NP}$ lacks both the twin-arginine signal and the associated transmembrane *rdhB* gene, suggesting it is a soluble cytoplasmic enzyme (Fig. 1a). *RdhA*$_{NP}$ is closely related in sequence to catabolic reductive dehalogenases15, and more distantly to the respiratory chlorophenol reductases (Extended data Fig. 1).

RdhA$_{NP}$ could be purified under aerobic conditions without detrimental effect on cofactor content or activity, and the UV-Vis spectrum of purified RdhA$_{NP}$ is similar to that previously reported for respiratory RdhAs8–12, with a distinct feature at 390 nm for the reduced sample that likely corresponds to the Cob(I)alamin species (Fig. 1b). EPR spectroscopy of aerobically purified RdhA$_{NP}$ in frozen solution reveals a five-coordinate 'base off' cob(II)alamin cofactor, while reduction of the sample leads to a 2x[4Fe-4S]$^{1+}$ signal (Extended data Fig. 2). This is similar to the membrane-associated RdhA enzymes. Spin quantitation leads to 0.82 Co(II) and 1.84 reduced 4Fe-4S clusters per RdhA$_{NP}$, in agreement with Co(I) estimation (Fig. 1b) and Fe quantification using bathophenanthroline. The enzyme catalyzes the reduction of *ortho*-halogenated phenolic compounds using either reduced methyl viologen (MV) or NADPH (via spinach ferredoxin and ferredoxin:NADP^{+} oxidoreductase) as electron donors (Fig. 1c). The latter reaction can be performed under aerobic conditions (Fig. 1d). RdhA$_{NP}$ displays a strict requirement for *o*-halogenated phenolic substrates, with a clear preference for those containing a 2,6-dihalogenated phenolic moiety. Highest activity was observed with 3,5-dibromo-4-hydroxybenzoic acid –a breakdown product of the herbicide bromoxynil (Fig. 1e).

To provide mechanistic insights and a structural basis for the observed substrate specificity, we determined the 2.3 Å crystal structure of RdhA$_{NP}$ (Extended data table 1). The structure reveals a compact globular fold with a central core domain responsible for cofactor binding (residues 244-606) that corresponds in size to the respiratory RdhA enzymes (Fig. 2a). The cobalamin cofactor is bound in the base-off form by a flavin-reductase like domain (residues 244-505), reminiscent of the human vitamin B12-processing enzyme CblC, the closest structural homolog available16 (Extended data Fig. 3a). The N-terminal domain (residues 1-243) represents a duplication and divergence of the cobalamin binding domain.

The cobalamin ligand is located at the extensive interface between the flavin-reductase domain and the C-terminal 2x[4Fe-4S] binding region, and is bound by 11 direct hydrogen bonds between the corrin ring and the protein (Fig. 2b). The base-off conformation of the

5,6-dimethylbenzimidazole (DMB) is stabilized by 4 direct hydrogen bonds (in addition to a network of water mediated polar interactions), an ionic interaction between the cobalamin phosphate and Lys542, and the stacking of the DMB moiety in between Pro461 and Tyr538. The Cβ of Asp476 is located directly below the Co ion (~5.5 Å), hindering binding of any solvent derived ligands. In contrast, the opposite side of the corrin ring is located at the bottom of a letter-box shaped cavity providing direct access to solvent (Fig. 2c).

The C-terminal region (506-694) consists of a series of alpha helices and extended loop regions that wrap around the functional cobalamin binding domain. The 505-606 stretch contains the bacterial 2x[4Fe-4S] ferredoxin-like motif and binds both [4Fe-4S] clusters, that are held approximately 9.8 Å apart (closest Fe-Fe distance) and are both located near the surface of the protein (Fig 2a,d). The first [4Fe-4S] cluster is linked by the first three cysteines of a typical bacterial CXXCXXCXXXCP ferredoxin motif and located approximately 12.4 Å from the cobalamin (nearest S-corrin ring distance). The second [4Fe-4S] cluster is located in direct van der Waals contact with the edge of B pyrrole from the corrin ring (Fig. 2d). In the latter case, the corresponding [4Fe-4S] binding motif contains a variable insertion between the first (Cys548) and second cysteine (Cys561) in the majority of reductive dehalogenases. Despite the fact that all cysteine ligands are conserved, this cluster is replaced in some reductive dehalogenases by a [3Fe-4S] cluster8–12. It is interesting to note that Cys548 is in direct van der Waals contact with the cobalamin (Extended data Fig 3b), with few exceptions17 Fe-S clusters are rarely in direct contact with porphyrin cofactors. This is suggestive of a link between FeS cluster maturation and cobalamin incorporation in reductive dehalogenases.

The reductive dehalogenase active site can clearly be identified as the solvent exposed cavity above the cobalamin plane (Fig. 2b,c). While we have been unable to determine the structure of a substrate-enzyme complex, docking of the relatively rigid 3,5-dibromo-4-hydroxybenzoic acid substrate leads to a plausible model whereby one of the substrate bromide atoms is located directly above the Co ion (Fig. 2e), in close contact with the side chains of Tyr426, Lys488 and Arg552. The substrate aromatic plane is orientated near perpendicular to the corrin ring, with the second bromide atom located in a hydrophobic cavity. The substrate hydroxyl group is in hydrogen bonding contact with Ser422, Lys488 and Arg552, suggesting it is bound in the deprotonated state. Close inspection of the electron density corresponding to a 5th ligand to the Co ion reveals it is best modeled by a chloride ion (Fig. 2b and Extended data Fig. 3c). Furthermore, low resolution RdhA$_{NP}$ structures of iodide containing crystals display difference densities at locations that correspond to those of the bromide atoms in the modelled substrate-enzyme complex (Extended data Fig. 3d).

EPR spectroscopic studies confirm the presence of a halogen-cobalamin interaction predicted by the substrate-enzyme model. Spectra of the type observed in Fig. 3a have been reported for various AdoCbl-dependent proteins18 and for cobinamides19 in solution, and typically arise from cob(II)alamin with water as the fifth axial ligand. Addition of NaCl to RdhA$_{NP}$ gave rise to the spectrum in Fig. 3b. While superficially resembling that of Fig. 3a, there are additional features in Fig. 3b arising from interaction of the unpaired electron with an additional nucleus having I = 3/2, resulting in a quartet of four lines. This indicates an

unexpected interaction of the unpaired electron with a coordinated chloride ion ($\mathbf{A}_{||}^{\mathbf{Cl}}$). The inclusion of KBr in place of NaCl gave the spectrum in Fig. 3c. Bromide interacting with the cob(II)alamin should give rise to two overlapped quartets with larger hyperfine splitting than is observed for Cl. However, the spectrum we observe displays a complex mixture of Co and Br (super)hyperfine couplings ($\mathbf{A}_{\perp}^{\mathbf{Co}}$ and $\mathbf{A}_{\perp}^{\mathbf{Br}}$) around $g_{\perp}$ and an unusually low $g_{||}$ with no detectable Br coupling. The same phenomenon has been reported for the iodo-cob(II)inamide complex in methanol18 and is a clear indication of a Br-cob(II)alamin interaction. Addition of the substrate 3,5-dibromo-4-hydroxybenzoic acid produces the spectrum in Fig. 3d, with overlapping contributions from Co and Br (super)hyperfine coupling around $g_{\perp}$ ($\mathbf{A}_{\perp}^{\mathbf{Co}}$ and $\mathbf{A}_{\perp}^{\mathbf{Br}}$) and also a complex, overlapped pattern of Br superhyperfine coupling in the parallel features ($\mathbf{A}_{||}^{\mathbf{Br}}$) that indicates unprecedented interaction of the unpaired electron on cob(II)alamin with a Br atom of the substrate. Addition of weaker binding substrates such as 3,5-dichloro-4-hydroxybenzoic acid gave rise to multiple species reflecting mobility within the active site (Extended data Fig. 4).

To further probe the effects of halogen-cobalt coordination, we carried out DFT calculations on an active site model (Extended data Fig. 5). These calculations suggest that substrate binding is likely to be stabilized by weak Co(II)-Br ligation and through hydrogen bonding of Lys488 and Arg552 to the substrate hydroxyl group. While the cobalamin-Br ligation is expected to be lost upon reduction to the Co(I) state, this is accompanied by an elongation of the substrate C-Br bond and a contraction of the Co-Br distance from 2.84 Å to 2.72 Å (Extended data Table 2).

Previous suggestions for the mechanism of reductive dehalogenase catalysis can be roughly divided into those invoking a transient organocobalt adduct and those favoring a radical mechanism13. The $RdhA_{NP}$ structure is incompatible with formation of an organocobalt adduct (Extended data Fig. 3e). The proposed radical mechanisms place fewer restraints on the relative position of Co and substrate, and therefore appear compatible with our structural data, although no direct evidence for a substrate radical has been obtained for RdhA enzymes. However, our structural and spectroscopic data suggest an alternative route, whereby the cobalamin is directly involved in halogen abstraction through formation of a halogen-cobalt bond.

Formation of a halogen-cob(II)alamin bond (as detected by EPR) drives catalysis, with the substrate bromide atom replacing the 5^{th} ligand prior to reductive dehalogenation. In this configuration, the conserved Tyr426/Lys488 dyad is ideally placed to act as a hydrogen donor to the halogenated carbon (Fig. 4). We propose the carbon-halogen bond could break either heterolytically, with transient formation of a halogen-Cob(III)alamin following nucleophilic attack by Co(I), or homolytically, following formation of an aryl radical through electron transfer from either the Co(I) or the adjacent [4Fe-4S] cluster. We show that mutation of Y426F or K488Q does not appear to affect corrinoid/[4Fe-4S] binding but abolishes enzyme activity, implicating both residues in the RdhA catalytic mechanism (Extended data Fig. 6). While the R552L $RdhA_{NP}$ variant also lacks activity, this variant has drastically altered properties.

Our proposed $RdhA_{NP}$ mechanism is fundamentally different from other B12-containing enzymes13–14 and from the hydrolytic dehalogenases, which use a direct S_N2-type attack on the substrate carbon20. In contrast, we propose the reductive dehalogenase uses the cobalamin cofactor to attack the substrate halogen atom itself, leading to C-halogen bond breakage concomitant with protonation of the leaving group. Distinct variations upon this theme could occur within the RdhA family to account for the varied substrate specificity (aliphatic versus aromatic organohalides) as well as the dihalo-elimination catalyzed by some enzymes21 (Extended data Fig. 7). The formation of a cobalamin-halide complex via oxidative addition to the Co ion is a new paradigm in both organohalide and cobalamin biochemistry and suggests the B12-biochemical repertoire is likely more varied than anticipated. In fact, recent studies hint at a distant enzyme relative being involved in tRNA modification22. Our findings should serve to guide future exploitation of the reductive dehalogenases.

Methods

Cloning of *N. pacificus rhdA$_{NP}$* for *B. megaterium* heterologous expression

A BLASTp search of the *Nitratireductor pacificus* pht-3B genome*23* using the protein sequence of *Comamonas* sp. 7D-2 BhbA (YP_007878394) revealed three putative reductive dehalogenase homologs sharing 72% (WP_008593084.1), 51% (WP_008595008.1) and 42% (WP_008597722.1) identity with BhbA. The *N. pacificus* WP_008597722.1 gene ($RdhA_{NP)}$ was shorter than the other homologs, lacking the putative C-terminal reductase domain. The *rdhA$_{NP}$* gene was codon optimized to remove codons that were rare in both *E. coli* and *B. megaterium* and synthesized (Genscript). *N. pacificus rdhA$_{NP}$* was PCR amplified using primers NPRdhA3pPT7F and NPRdhA3pPT7R (the latter containing the sequence encoding for a C-terminal His-tag) using Phusion polymerase (NEB). The PCR product was cloned into the *Bsr*GI and *Bam*HI sites of pP_{T7} plasmid24 using Infusion HD (Clontech) and transformed into *E. coli* NEB5α. Once the sequence of the insert was confirmed the purified plasmid was transformed into *B. megaterium* MS941 containing the pT7-RNAP plasmid that permits xylose inducible expression of T7 polymerase23, using the modified minimal medium protoplast transformation protocol25.

Mutagenesis

Mutagenesis primers were designed using the QuikChange® Primer Design Program (http://www.genomics.agilent.com/primerDesignProgram.jsp). PCR was performed using Phusion polymerase (NEB). Template was removed by *Dpn*I (NEB) digest and the PCR product transformed into *E. coli* NEB5α. Once the presence of the desired mutation was confirmed by DNA sequencing, the plasmid was transformed into *B. megaterium* as above.

Heterologous expression of *rdhA$_{NP}$* WT and mutants in *B. megaterium*

B. megaterium transformants were grown in 1 L LB supplemented with 10 μg/mL tetracycline and 4.5 μg/mL chloramphenicol at 37 °C/180 rpm until the culture reached an OD_{578} ~0.4. Cultures were supplemented with 50 μM ammonium iron(II) sulfate, 1 μM B12 and induced with 0.1% xylose. Cultures were grown overnight at 17 °C/180 rpm and then harvested by centrifugation (4 °C, 7000 *g* for 10 minutes).

Purification of $RdhA_{NP}$ WT and variant enzymes

Cell pellets were resuspended in buffer A (200 mM NaCl, 50 mM Tris pH 7.5) supplemented with DNase, RNase, lysozyme (Sigma) and a Complete EDTA-free protease inhibitor cocktail (Roche). Cells were lysed using a French press at 1500 psi and the lysate clarified by centrifugation at 125,000 *g* for 90 minutes. The supernatant was applied to a Ni-NTA agarose column (Qiagen). The column washed successively with 3 column volumes of buffer A supplemented with 10 mM and 40 mM imidazole and protein eluted in 1 mL fractions with buffer A supplemented with 250 mM imidazole. Samples were subjected to SDS-PAGE analysis and fractions found to contain the purified protein were pooled. Imidazole was removed using a 10-DG desalting column (Bio-Rad) equilibrated with buffer A. Protein was concentrated as required using a Vivaspin centrifugal device (Sartorius).

UV-Vis spectroscopy/protein quantification

UV-Vis absorbance spectra were recorded with a Cary UV–Vis spectrophotometer. To obtain the reduced $RdhA_{NP}$ spectrum, 79 μM enzyme was incubated anaerobically with 25 μM 5-deazariboflavin and 2 mM EDTA under a blue LED lamp for 1 hour. Protein concentration was estimated using ε_{280} = 77810 M^{-1} cm^{-1} (calculated from the primary amino acid sequence using the ProtParam program on the ExPASy proteomics server).

Metal estimations

The iron content of RdhA was confirmed colourimetrically with bathophenanthroline after acid denaturation. Protein was mixed with an equal volume of 2M HCl and heated at 80 °C for ten minutes prior to the removal of the precipitate by centrifugation. A suitable volume of the supernatant was taken for analysis and made up to a final volume of 0.75 mL with water. Samples were mixed after addition of 0.2 mL saturated ammonium acetate. Sodium metabisulphite (0.1 M, 0.05 mL) and bathophenanthroline (0.1 M, 0.01 mL) were added and samples incubated at room temperature for ten minutes before reading the absorbance at 535 nm. Concentrations were determined from an iron standard curve measured over the range 0-50 nmoles.

Methyl viologen (MV) spectrophotometric activity assay

Purified $RdhA_{NP}$ was buffer exchanged into 50 mM Tris, pH 7.5, 200 mM NaCl under anaerobic conditions in a glove box (Belle Technology, UK). A 30 mM methyl viologen solution reduced by titration with sodium dithionite was prepared for the assay. The substrate dependent oxidation of dithionite-reduced methyl viologen was measured at 578 nm (ε = 978 mM^{-1} cm^{-1}). Screening of different organohalide compounds was performed by adding 100 μM of the substrate to the reaction mixture containing 2 μM enzyme in 50 mM Tris, pH 7.5, 200 mM NaCl and 300 μM dithionite-reduced methyl viologen. Oxidation of methyl viologen was measured for a period of 10 min and fit to a linear rate where appropriate. Full steady state characterization was done for 3,5-dibromo-4-hydroxybenzoic acid or 3,5-dichloro-4-hydroxybenzoic acid respectively, and a plot of the observed rate constant versus substrate concentration was fitted to a Michaelis-Menten steady-state model.

$RdhA_{NP}$ spinach ferredoxin and ferredoxin:$NADP^+$ oxidoreductase assay

Reactions using spinach ferredoxin and ferredoxin:$NADP^+$ oxidoreductase were carried out either in an anaerobic glove box (Belle Technology, UK) or under aerobic conditions. For anaerobic assays purified $RdhA_{NP}$ was buffer exchanged into 50 mM Tris, pH 7.5, 200 mM NaCl under strict anaerobic conditions. Reactions contained 100 nM $RdhA_{NP}$, 200 μM NADPH, spinach ferredoxin and ferredoxin:$NADP^+$ oxidoreductase in an enzyme ratio of 1:10:2 ($RdhA_{NP}$:ferredoxin:ferredoxin $NADP^+$ oxidoreductase). All assays were initiated by the addition of 2 mM 3,5-dibromo-4-hydroxybenzoic acid. Following incubation for 1 hr, reactions were stopped by rapid freezing in liquid nitrogen and analyzed by HPLC.

HPLC assays

Sample analysis was performed using an Agilent 1100 Series HPLC equipped with a UV detector. The stationary phase was a Kinetex 5μ C18 100A column, 250 × 4.6 mm. The mobile phase was acetonitrile/water (50/50) with 0.1 % TFA at a flow rate of 1 mL/min, and detection was performed at a wavelength of 264 nm.

Crystallization

Purified $RdhA_{NP}$ protein in 50 mM Tris, pH 7.5, 200 mM NaCl was concentrated in a Vivaspin 30 kDa cut off spin concentrator to a final concentration of 11 mg/mL. Initial screening mixing 0.25 μL protein with 0.25 μL mother liquor led to small crystals in a variety of conditions when incubated at 4° C. Crystals obtained with 0.2 M sodium iodide, 0.1 M Bis Tris propane, 20% w/v PEG3350 were used to prepare a seed stock, and a second screening was carried out by mixing 0.25 μL protein plus 0.05 μL seed stock with 0.3 μL screen buffer. Crystals were obtained with 0.2 M potassium thiocyanate, 0.1 M sodium cacodylate pH 6.5, 8% w/v PEG 20K plus 8% v/v PEG550MME when incubating at 4° C.

Diffraction data collection and structure elucidation

Crystals were flash-cooled in liquid nitrogen by supplementing the mother liquor with 10% PEG 200. Data were collected at Diamond beamlines at 100K and subsequently handled using the CCP4 suite26. All data were reduced and scaled using XDS27 and initial phases obtained by merging various native datasets (all collected at 0.9795 Å wavelength) using BLEND26. This generated a highly redundant low-resolution data set with sufficient anomalous signal from the native Fe and Co ions to allow substructure determination using Shelx28 and initial phasing using MLPHARE26. Interpretable maps were obtained following density modification and three-fold NCS averaging combined with phase extension to 2.8 Å using DM26. An initial model was automatically generated using ArpWarp29, and iteratively rebuilt and refined against a single high resolution data set using Coot and REFMAC526. The final model was refined using data extending to 2.3 Å and contains 3 molecules in the asymmetric unit. While the identity of the 5^{th} ligand to the Co-ion could not be unambiguously established from the X-ray data alone, modeling this as a chloride ion resulted in the most plausible model and is in agreement with our EPR-spectroscopic data (when refining this as a water ligand, individual B factors for the water ligand were lower than that of the corresponding Cobalt ion for all three monomers in the AU). A low resolution data set (to 3.5 Å) of an $RdhA_{NP}$ crystal obtained in the presence of

200mM sodium iodide was used to determine position of iodide sites using difference Fourier methods. For final data and refinement statistics see Extended data Table 1. Ramachandran statistics of the model show 96.93% in the favored and 2.54% in the allowed regions.

EPR spectroscopy

Experimental parameters: microwave power 0.5 mW, modulation frequency 100 kHz, modulation amplitude 5 G, temperature 30 K. Spectra were obtained using a Bruker ELEXSYS E500 spectrometer, Super high Q resonator (ER 4122SHQ), Oxford Instruments ESR900 cryostat and ITC503 temperature controller. Cob(II)alamin contains a low spin, S = ½ (i.e. one unpaired electron), ion with electronic configuration [Ar]3d7. The unpaired electron is in the d_z2 orbital and this leads to axial spectra that can be described by two *g* values and two cobalt hyperfine values ($\mathbf{A^{Co}}$), each designated parallel (||) and perpendicular (⊥). The latter describe the (hyperfine) interaction of the single unpaired electron with the nuclear magnetic moment of the cobalt ion. The cobalt nucleus has nuclear spin I = 7/2 and thus splits the spectrum into eight lines. In five coordinate base-off complexes as described here, the hyperfine and g tensors are not collinear in x and y and this together with dislocation strain leads to a lack of resolution in the $A_\perp$ lines. The additional features in Fig. 3b arise from interaction of the unpaired electron with an additional nucleus having I = 3/2, giving rise to a quartet of four lines. This indicates an unprecedented interaction of the unpaired electron with a coordinated chloride ion, chlorine has I = 3/2 and over 75% of natural chlorine is the ^{35}Cl isotope, leading to a chlorine superhyperfine interaction ($\mathbf{A_{||}^{Cl}}$). Bromine exists as two isotopes, ^{79}Br and ^{81}Br, in essentially a 1:1 ratio, each having I = 3/2 but differing in magnetic moment by ~ 7.5% and with even the smaller of the two magnetic moments being ~ 2.5 times greater than that of Cl. Thus bromide interacting with the cob(II)alamin should give rise to two overlapped quartets with larger hyperfine splitting than is observed for Cl. The concentrations of EPR-detectable Co(II) and reduced 4Fe-4S clusters were estimated by double integration of the X-band continuous wave EPR signals of these species recorded at non-saturating microwave powers and comparison of these double integrals with that of a Cu(II) standard of known concentration recorded under the same conditions. Error estimated at +/− 5%

Docking

Computational docking of the substrate 3,5-dibromo-4-hydroxybenzoic acid to $RdhA_{NP}$ was performed using AutoDock vina30. A doubly-deprotonated substrate model was optimized using the UFF force field with Gaussian 0931. AutoDock Tools 1.5.632 was used to assign hydrogens and Gasteiger charges to $RdhA_{NP}$. The substrate carboxy moiety was made rotatable, and the four residues Phe291, Tyr426, Lys488 and Arg 552 were made flexible. A docking grid with dimensions of 24 × 36 × 18 Å was used to include the entire active site/ substrate binding cavity. The final docking conformation was chosen based on the conformation with the shortest substrate heavy atom to cobalamin Co distance. This conformation was 1.4 kcal/mol higher in energy than the highest scoring result.

Density functional theory (DFT) calculations

A DFT active site model based on the crystal structure of $RdhA_{NP}$ with docked substrate was optimized using the (U)BP86/6-31G(d,p) level of theory implemented in Gaussian 0931. The BP86 functional has been shown to be the most appropriate for the prediction of both structural and electronic properties of B12 cofactors (ref *33* and references within). The model consists of a 'trimmed' tetracoordinate cobalamin, the truncated side chains of Tyr426, Lys488, Arg552 and the substrate analog 2,6-dibromo-4-methylphenol, which was deprotonated (Extended data Fig. 5). Four atoms, including the cobalamin Co, were fixed during optimization. The Co(I), Co(II) and Co(III) oxidation states were examined and Br^--ligated cobalamin models were also examined for comparison of the Co-Br bond lengths.

Extended Data

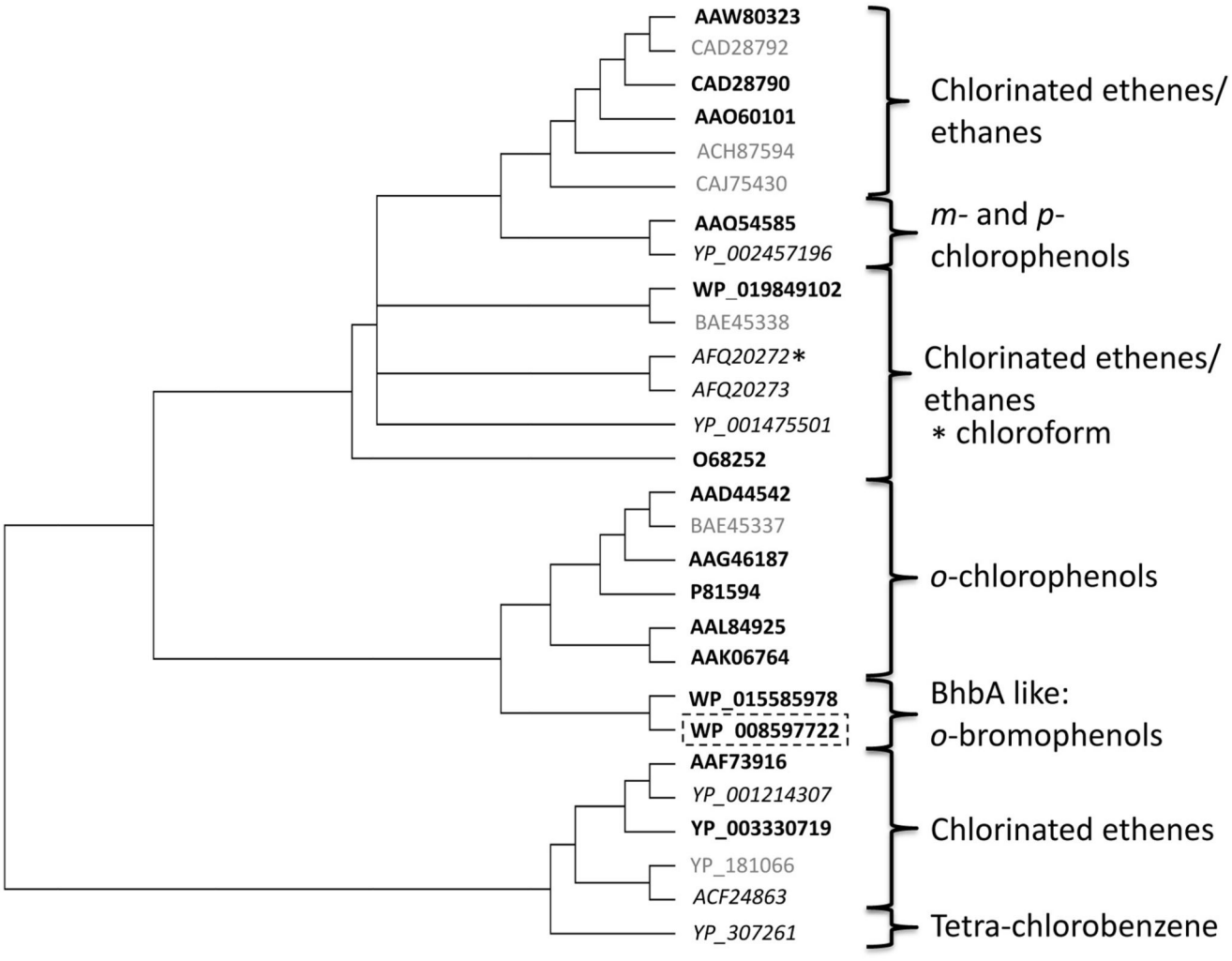

ED Fig. 1. Phylogenetic tree of functionally characterized reductive dehalogenases (RdhAs). Those in bold have been purified and characterised *in vitro*. Those in italics have been identified from crude lysate assays via native PAGE or knock out/knock in. Those in plain

text have implied substrate range based on transcriptional regulation. The sequence accession codes are as follows, AAD44542 = *Desulfitobacterium dehalogenans* ATCC 51507 CprA, P81594 = *Desulfitobacterium hafniense* DCB-2 CprA1, AAQ54585 = *Desulfitobacterium hafniense* PCP-1 CprA5, AAL84925 = *Desulfitobacterium chlororespirans* CprA, WP_019849102 = *Desulfitobacterium sp*. PCE-1, AAK06764 = *Desulfitobacterium hafniense* PCP-1 CprA3, AAO60101 = *Desulfitobacterium hafniense* PCE-S PceA, O68252 = *Dehalospirillum multivorans* PceA, AAF73916 = *Dehalococcoides mccartyi* TceA, YP_181066 = *Dehalococcoides mccartyi* 195 PceA, AAW80323 = *Desulfitobacterium hafniense* Y51 PceA, CAD28790 = *Dehalobacter restrictus* PceA, CAD28792 = *Desulfitobacterium hafniense* TCE1 PceA, YP_001214307 = *Dehalococcoides mccartyi* BAV1 BvcA, YP_003330719 = *Dehalococcoides mccartyi* VS VcrA, ACF24863 = *Dehalococcoides sp*. MB MbrA, YP_307261 = *Dehalococcoides mccartyi* CBDB1 CbrA, BAE45338 = *Desulfitobacterium sp*. KBC1 PrdA, BAE45337 = *Desulfitobacterium sp*. KBC1 CprA, ACH87594 = *Dehalobacter sp*. WL DcaA, CAJ75430 = *Desulfitobacterium dichloroeliminans* LMG P-21439 DcaA, AFQ20272 = *Dehalobacter sp*. CF CfrA , AFQ20273 = *Dehalobacter sp*. DCA DcrA , AAG46187 = *Desulfitobacterium sp.* PCE1 CprA, YP_002457196 = *Desulfitobacterium hafniense* DCB-2 RdhA3 , YP_001475501 = *Shewanella sediminis* HAW-EB3 PceA, WP_015585978 = *Comamonas sp*. 7D-2 BhbA, WP_008597722 = *Nitratireductor pacificus* $RdhA_{NP}$

Europe PMC Funders Author Manuscripts

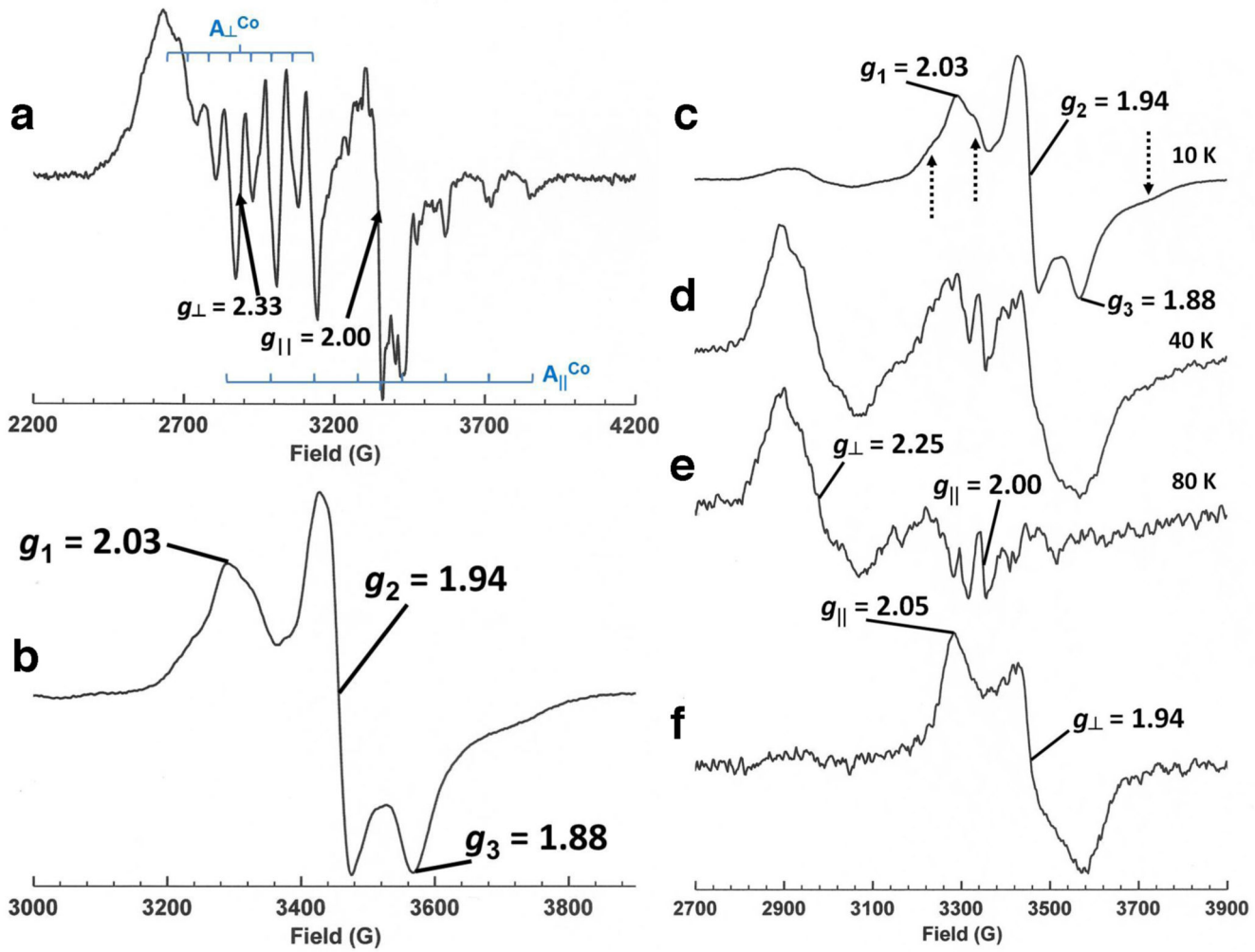

ED Fig. 2. EPR spectroscopic analysis of reduced $RdhA_{NP}$ (79μM).

Left panel X-band EPR spectra of $RdhA_{NP}$ (**a**) as isolated, 150 μM (**b**) reduced using EDTA, deazaflavin and light, 79 μM. **Right panel (c)** X-band (~9.39 GHz) continuous wave EPR spectrum of reduced $RdhA_{NP}$ recorded at 10 K showing a 2x$[4Fe\text{-}4S]^{1+}$ signal indicative of two magnetically interacting 4Fe-4S clusters due to features marked ⇢ ; *g* values marked for rhombic $[4Fe\text{-}4S]^{1+}$ signal. **(d)** X-band continuous wave EPR spectrum of reduced $RdhA_{NP}$ at 40 K. **(e)** X-band continuous wave EPR spectrum of reduced $RdhA_{NP}$ at 80 K showing small base-on cob(II)alamin signal with *g* values marked. **(f)** Subtraction of (e) from (d) reveals a second axial $[4Fe\text{-}4S]^{1+}$ signal, with *g* values as marked, demonstrating that we can observe EPR signals from two different 4Fe-4S clusters within $RdhA_{NP}$. Experimental parameters, microwave power 0.5 mW, field modulation frequency 100 KHz, field modulation amplitude 7 G, temperatures as given.

Europe PMC Funders Author Manuscripts

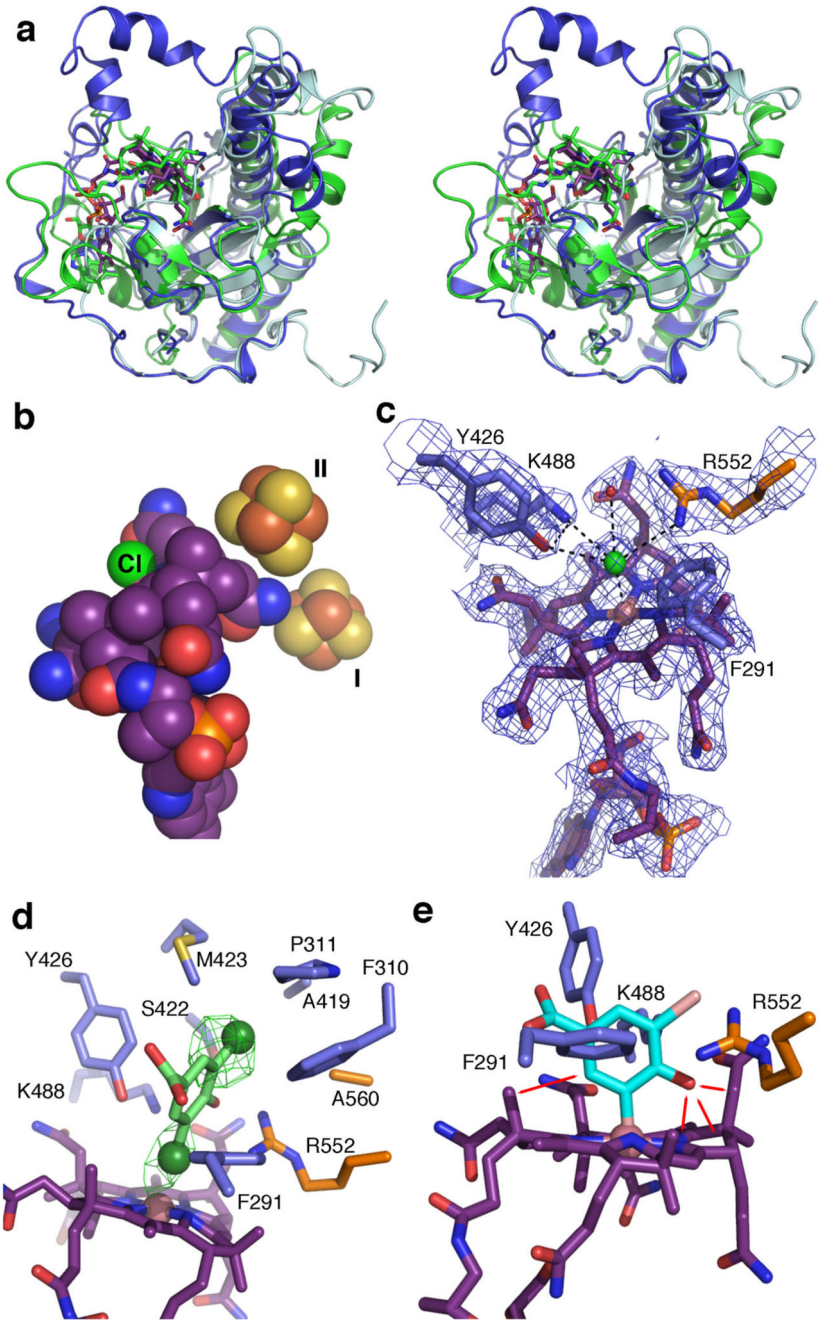

ED Fig. 3. Crystal structure of RdhA$_{NP}$.

(a) Stereo view of an overlay of the RdhA$_{NP}$ cobalamin-binding domain (in blue), the N-terminal non-functional cobalamin binding domain (in light blue) and the human vitamin B12-processing enzyme CblC (in green). The cobalamin cofactor is bound in a similar base-off manner by both RdhA$_{NP}$ and CblC. The RdhA$_{NP}$ non-functional cobalamin binding domain does contain an irregular water filled cavity corresponding to the cofactor binding site, but no longer contains any of the residues implied in cofactor binding. **(b)** Representation of the RdhA$_{NP}$ cofactors in space filling spheres. The second [4Fe-4S]

cluster is in van der Waals contact with the corrin ring, the B pyrrol *d*-amide corrin moiety is lined along one side of the cluster and forms a hydrogen bond to one of the S-ions. **(c)** Detailed view of the $RdhA_{NP}$ 5th ligand binding site. Residues in close contact with the chloride ligand are shown in atom colored sticks (color coded as in Fig 2). The $2F_o$-F_c map is contoured at 1 sigma and shown as a blue mesh. The Tyr426-Lys488 distance is 2.7 Å. **(d)** Model of the $RdhA_{NP}$-substrate complex (color coded as in the main manuscript, Fig 2e) with the F_oF_c-omit map for an iodide-soaked crystal (to 3.5 Å; contoured at 6 sigma) depicted by a green mesh. Difference density can be clearly seen at positions corresponding to those predicted to accommodate the bromide atoms of the substrate. **(e)** Putative structure of an organometallic substrate-cobalamin intermediate within the $RdhA_{NP}$ active site. The substrate was positioned to minimize close contacts with active site residues. Severe clashes can be observed between the substrate and the corrin ring (highlighted by red lines).

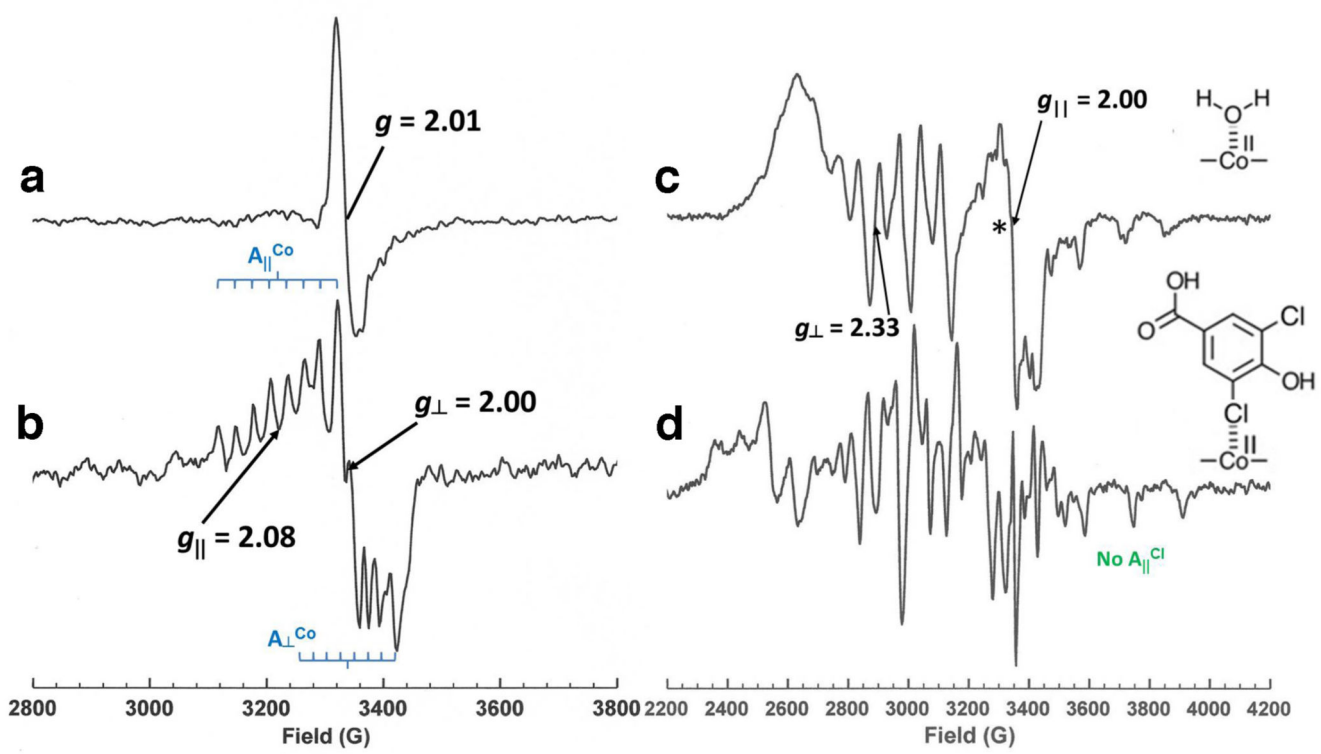

ED Fig. 4. Additional EPR spectroscopic data.

Left panel Identification of contaminating EPR signals in aerobically purified $RdhA_{NP}$ (150μM). (**a**) X-band continuous wave EPR spectrum showing a $[3Fe\text{-}4S]^{1+}$ cluster signal isolated by subtraction of the spectrum recorded at 20 K from that recorded at 12 K. (**b**) X-band continuous wave EPR spectrum showing cob(III)alamin-$O_2^{\bullet-}$ (superoxide) signal isolated by subtracting the spectrum recorded at 20 K from that recorded at 30 K followed by subtraction of a proportion of the $[3Fe\text{-}4S]^{1+}$ signal. Neither of these signals quantitates to more than 4% of the total EPR signal in the protein as isolated. Experimental parameters, microwave power 0.5 mW, field modulation frequency 100 KHz, field modulation amplitude 5 G, temperatures as given. **Right panel.** Binding of 3,5-dichloro-4-hydroxybenzoate to 150μM $RdhA_{NP}$ leads to a spectrum exhibiting multiple $A_{\perp}^{Co}$ and $A_{||}^{Co}$ splitting of the

spectrum and no apparent chlorine superhyperfine coupling ($A_{||}^{Cl}$) (spectrum **d**). This suggests relatively disordered binding and possibly substrate movement within the active site on the nanosecond time scale even at the cryogenic temperatures employed in the EPR experiment. Such disorder and dynamics may explain the poor efficacy of this substrate relative to the dibromo- analogue (see main Fig. 1E) in addition to precluding analysis of the EPR spectrum.

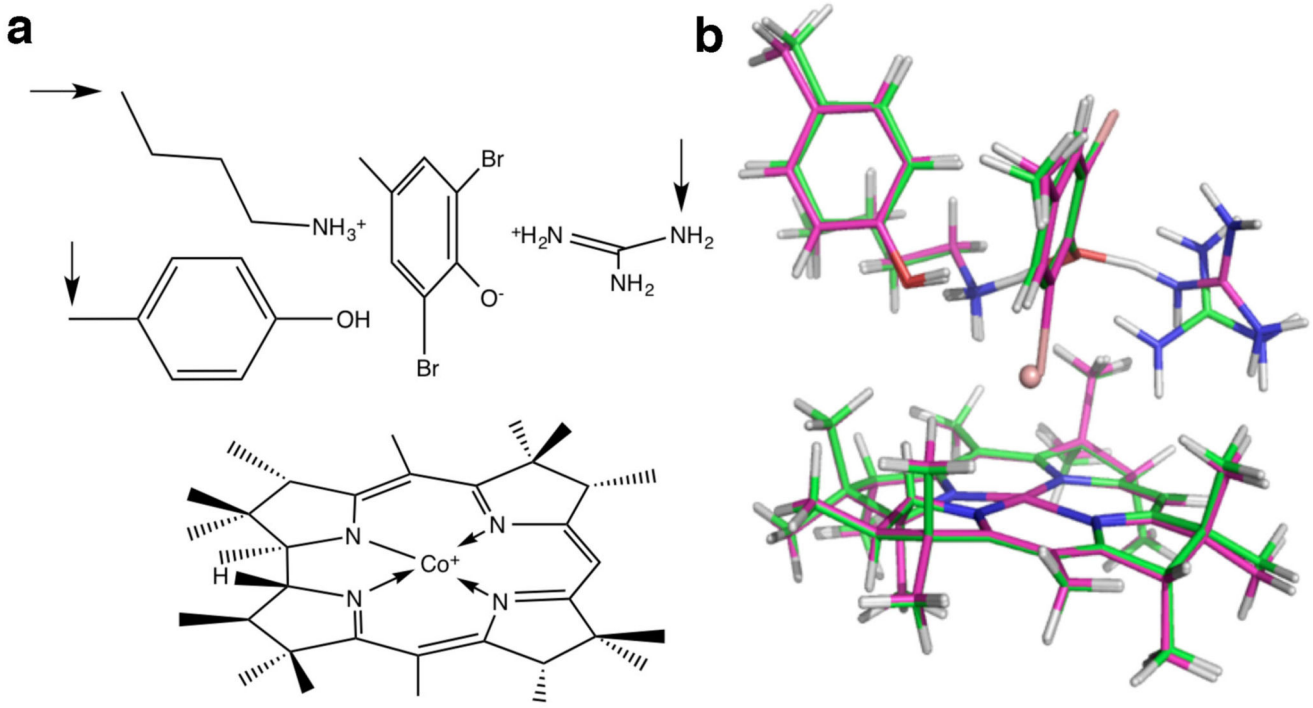

ED Fig. 5. Structure of the RdhA$_{NP}$ active site DTF model.

a) Chemical structures used for DFT calculations and **b)** overlay of the optimized active site models in the Co(II) (pink carbons) and Co(I) (green carbons; Br is shown as discrete sphere) oxidation states (right panel). The Co and the 3 atoms indicated with arrows (**a**) were fixed during optimisation. Selected parameters are given in Extended data Table 2 and Cartesian coordinates of the optimised structures are included in the Supplementary material. The Cbl-Br models comprise the 'trimmed' cobalamin with a single axial Br ligand and contain 91 atoms (40 heavy atoms). The full active site model contains 148 atoms (66 heavy atoms).

Europe PMC Funders Author Manuscripts

Europe PMC Funders Author Manuscripts

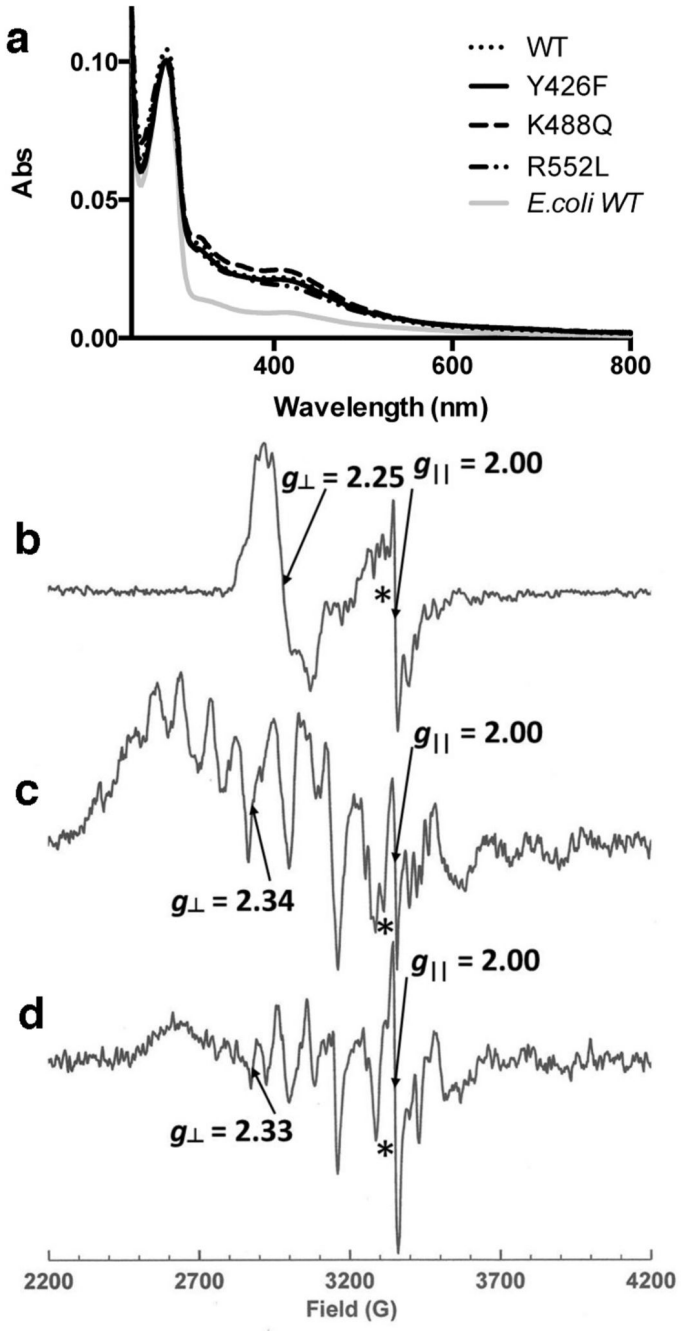

ED Fig. 6. Characterisation of RdhA$_{NP}$ mutants.

a) UV-Vis spectra of RdhA$_{NP}$ variants normalised using the A$_{280}$ absorbance. Mutants Y426F (107 μM), K488Q (100 μM) and R552L (95 μM) have a similar profile as the wild type enzyme (WT, 176 μM) purified from *B. megaterium*. RdhA$_{NP}$ WT purified from *E. coli* (lacking the corrinoid cofactor; 250 μM) is shown for comparison. **b-c-d)** Continuous wave X-band EPR at 30K for RdhA$_{NP}$ mutants. (**b**) R552L mutant (75 μM), (**c**) K488Q mutant (65 μM) and (**d**) Y426F mutant (65 μM). Each shows the presence of cob(II)alamin which is

base on in R552L and base off in the other two mutants. Experimental parameters: microwave power 0.5 mW, modulation frequency 100 KHz, modulation amplitude 7G.

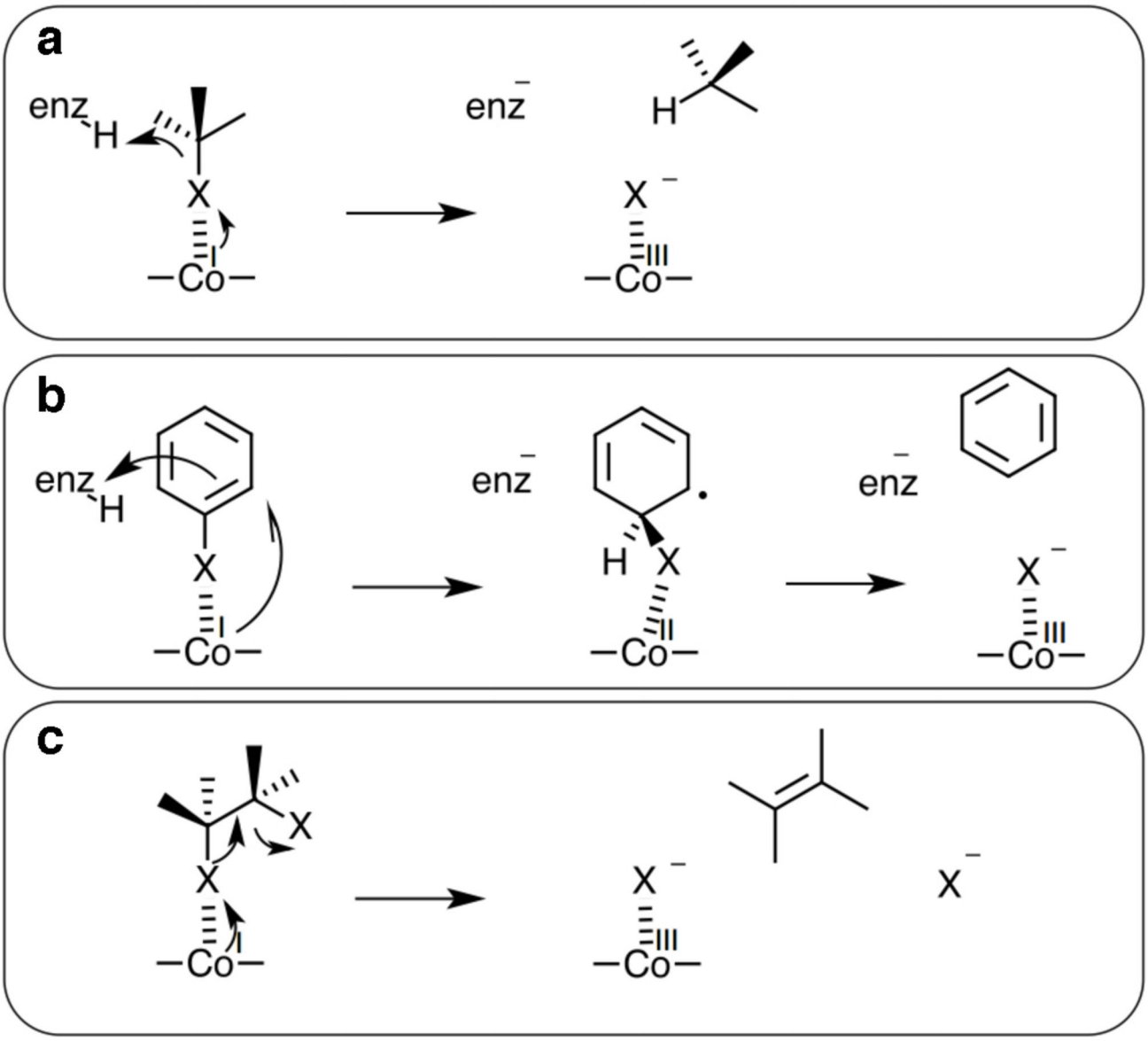

ED Fig. 7. Mechanistic proposal for biological reductive dehalogenation.

Our proposed $RdhA_{NP}$ mechanism is fundamentally different from those for other B12-containing enzymes13,14, but also differs from the hydrolytic dehalogenases, which use an S_N2 mechanism whereby either an activated water molecule or a catalytic Asp residue attacks the substrate carbon5. The latter contain a specific halogen binding site that is believed to contribute to stabilization of the transition state and to facilitate departure of the halide leaving group. In contrast, we propose the reductive dehalogenase uses the cobalamin cofactor to attack the substrate halogen atom itself, leading to C-halogen bond breakage concomitant with protonation of the leaving group. Distinct variations upon this theme could

occur within the RdhA family: aliphatic organohalide reductases could operate via heterolytic C-halogen bond cleavage concomitant with halogen-Co(III) bond formation and substrate protonation (panel **a**). Those acting on (unactivated) aromatic organohalides are likely to operate via a radical substrate intermediate using homolytic C-halogen bond cleavage (panel **b**), while certain reductive dehalogenases have been shown to catalyse vicinal reduction or dihalo-elimination, and we propose formation of the Co-halogen bond occurs concomitant with leaving of the vicinal halogen atom (panel **c**).

Extended Data Table 1

Data collection, phasing and refinement statistics

	$RdhA_{NP}$*
Data collection	
Space group	C2
Cell dimensions	
a, *b*, *c* (Å)	177.34, 171.51, 109.02
α, *β*, *γ* (°)	90, 98.87, 90
Resolution (Å)	76.9-2.3 (2.36-2.3)**
R_{pim}	6.0 (65.0)
$I/\sigma I$	9.2 (1.5)
Completeness (%)	98.8 (99.6)
Redundancy	3.3 (3.2)
Refinement	
Resolution (Å)	76.9-2.3 (2.36-2.3)
No. reflections	133721 (9993)
R_{work}/ R_{free}	18.2/20.66 (31.2/35.4)
No. atoms	
Protein	16149
Ion	6
Water	267
B-factors	
Protein	25.4
Ligand/ion	49.1
Water	45.5
R.m.s deviations	
Bond lengths (Å)	0.020
Bond angles (°)	2.07

Extended data Table 2

Selected parameters obtained from DFT calculations of model compounds

		Substrate[a]	Cbl-Br[b]			Active site model[f]	
			Co(I)	Co(II)	Co(III)	Co(I)	Co(II)
energy, Ha		**-5488.955**	**-5500.405**	**-5500.371**	**-5500.191**	**-9184.368**	**-9184.097**
Total atomic charges	Total	-1	-1	0	1	1	2
	Co		0.56	0.67	0.67	0.58	0.72
	Br		-0.76	-0.41	-0.15	-0.06	-0.05
	Cbl		-0.81	-0.26	0.48	-0.82	-0.21
	Substrate[c]					-0.16	-0.02
	Active site[c]					1.47	1.55
Total spin density	Total	0	0	1	0	0	1
	Co			0.89			1.02
	Br			0.22			0
	Cbl[c]			-0.11			-0.04
	Substrate[c]						0.02
	Active site[c]						0
Bond length[d], Å	Co-Br		5.19[e]	2.53	2.30	2.72	2.84
	C_{S1}-Br	1.94				2.02	1.96
	C_{S3}-Br					1.92	1.92
	C_{S2}-O_S					1.34	1.33
	O_Y-C_{S1}					3.11	3.17
	N_K-O_S					2.63	2.59
	N_R-O_S					2.67	2.59
Angle,°	Co-Br-C_{S1}					174.3	178.2

Extended Data Table 3

EPR parameters for the spectra shown in Figure 3

Ligand	$g_{\perp}$	Co(II) $A_{\perp}$(G)	$g_{\parallel}$	Co(II) $A_{\parallel}$ (G)	Ligand $A_{\parallel}$ (G)
H_2O	2.33	70	2.00	143	-
Cl^-	2.33	71	2.00	143	25.4
Br^-	2.30	79*	1.88	139	-
3,5-dibromo-4-hydroxybenzoic acid	2.37	82*	2.00	160	39, 35

Supplementary Material

Refer to Web version on PubMed Central for supplementary material.

Acknowledgments

This work was supported by an ERC grant (DEHALORES206080) to D.L. S.H. is a BBSRC David Phillips research fellow. C.Q. is supported by CONICYT Chile. We thank Diamond Light Source for access to beamline IO4 (proposal number MX8997) that contributed to the results presented here; R. Biedendieck (Technische Universität Braunschweig, Germany), S. Moore and M. Warren (University of Kent, UK) for providing plasmids and assistance with B. megaterium molecular biology; the assistance given by IT Services and the use of the Computational Shared Facility at The University of Manchester and A. Munro (University of Manchester) for critical comments and discussion.

References

1. Stringer, Ruth; Johnston, Paul, editors. Chlorine and the Environment: An overview of the chlorine industry. Dordrecht, the Netherlands: Kluwer Academic; 2001. p. 448ISBN 0792367979
2. Oberg G. The natural chlorine cycle--fitting the scattered pieces. Appl Microbiol Biotechnol. 2002; 58:565–81. [PubMed: 11956738]
3. Gribble GW. Occurrence of halogenated alkaloids. Alkaloids Chem Biol. 2012; 71:1–165. [PubMed: 23189746]
4. Smidt H, de Vos WM. Anaerobic microbial dehalogenation. Annu Rev Microbiol. 2004; 58:43–73. [PubMed: 15487929]
5. Leys D, Adrian L, Smidt H. Organohalide respiration: microbes breathing chlorinated molecules. Philos Trans R Soc Lond B Biol Sci. 2013; 368(1616) 20120316. doi: 10.1098/rstb.2012.0316
6. Adrian L, Szewzyk U, Wecke J, Görisch H. Bacterial dehalorespiration with chlorinated benzenes. Nature. 2000; 408:580–58. [PubMed: 11117744]
7. Bunge M, et al. Reductive dehalogenation of chlorinated dioxins by an anaerobic bacterium. Nature. 2003; 421:357–360. [PubMed: 12540897]
8. Wohlfarth G, Diekert G. Anaerobic dehalogenases. Curr Opin Biotechnol. 1997; 8:290–295. [PubMed: 9206009]
9. van de Pas BA, et al. Purification and molecular characterization of ortho-chlorophenol reductive dehalogenase, a key enzyme of halorespiration in *Desulfitobacterium dehalogenans*. J Biol Chem. 1999; 274:20287–20292. [PubMed: 10400648]
10. Krasotkina J, Walters T, Maruya KA, Ragsdale SW. Characterization of the B12- and iron-sulfur-containing reductive dehalogenase from *Desulfitobacterium chlororespirans*. J Biol Chem. 2001; 276:40991–40997. [PubMed: 11533062]
11. Neumann A, et al. Tetrachloroethene reductive dehalogenase of *Dehalospirillum multivorans*: substrate specificity of the native enzyme and its corrinoid cofactor. Arch Microbiol. 2002; 177:420–426. [PubMed: 11976751]
12. Maillard J, et al. Characterization of the corrinoid iron-sulfur protein tetrachloroethene reductive dehalogenase of *Dehalobacter restrictus*. Appl Environ Microbiol. 2003; 69:4628–4638. [PubMed: 12902251]
13. Banerjee R, Ragsdale SW. The many faces of vitamin B12: catalysis by cobalamin-dependent enzymes. Annu Rev Biochem. 2003; 72:209–247. [PubMed: 14527323]
14. Brown KL. Chemistry and enzymology of vitamin B12. Chem Rev. 2005; 105:2075–2149. [PubMed: 15941210]
15. Chen K, et al. Molecular characterization of the enzymes involved in the degradation of a brominated aromatic herbicide. Mol Microbiol. 2013; 89:1121–1139. [PubMed: 23859214]
16. Koutmos M, Gherasim C, Smith JL, Banerjee R. Structural basis of multifunctionality in a vitamin B12-processing enzyme. J Biol Chem. 2011; 286:29780–29787. [PubMed: 21697092]
17. Stroupe, ME.; Getzoff, ED. The role of siroheme in sulfite and nitrite reductases. Tetrapyrroles: Their Birth, Life, and Death. Warren, MJ.; Smith, A., editors. Landes Bioscience; New York: 2005. p. 373-387.
18. Van Doorslaer S, et al. Axial solvent coordination in "base-off" cob(II)alamin and related co(II)-corrinates revealed by 2D-EPR. J Am Chem Soc. 2003; 125:5915–5927. [PubMed: 12733932]

19. Bayston JH, Looney FH, Pilbrow JR, Winfield ME. Electron paramagnetic resonance studies of cob(II)alamin and cob(II)inamides. Biochemistry. 1970; 9:2164–2172. [PubMed: 4315132]
20. de Jong RM, Dijkstra BW. Structure and mechanism of bacterial dehalogenases: different ways to cleave a carbon-halogen bond. Curr Opin Struct Biol. 2003; 13:722–30. [PubMed: 14675551]
21. Grostern A, Edwards EA. Characterization of a *Dehalobacter* coculture that dechlorinates 1,2-dichloroethane to ethene and identification of the putative reductive dehalogenase gene. Appl Environ Microbiol. 2009; 75:2684–93. [PubMed: 19270140]
22. Miles ZD, McCarty RM, Molnar G, Bandarian V. Discovery of epoxyqueuosine (oQ) reductase reveals parallels between halorespiration and tRNA modification. Proc Natl Acad Sci USA. 2011; 108:7368–72. [PubMed: 21502530]
23. Lai Q, Li G, Shao Z. Genome sequence of *Nitratireductor pacificus* type strain pht-3B. J Bacteriol. 2012; 194:6958. [PubMed: 23209217]
24. Gamer M, et al. A T7 RNA polymerase-dependent gene expression system for *Bacillus megaterium*. Appl Microbiol Biotechnol. 2009; 82:1195–1203. [PubMed: 19308404]
25. Moore SJ, et al. Elucidation of the anaerobic pathway for the corrin component of cobalamin (vitamin B12). Proc Natl Acad Sci USA. 2013; 110:14906–14911. [PubMed: 23922391]
26. Winn MD, et al. Overview of the CCP4 suite and current developments. Acta Crystallogr. 2011; D67:235–242.
27. Kabsch W. XDS. Acta Crystallogr. 2010; D66:125–132.
28. Sheldrick GM. Experimental phasing with SHELXC/D/E: combining chain tracing with density modification. Acta Crystallogr. 2010; D66:479–485.
29. Langer G, et al. Automated molecular model building for X-ray crystallography using ARP/Warp version 7. Nature Protocols. 2008; 3:1171–1179. [PubMed: 18600222]
30. Trott O, Olson AJ. AutoDock Vina: improving the speed and accuracy of docking with a new scoring function, efficient optimization and multithreading. J Comput Chem. 2010; 31:455–461. [PubMed: 19499576]
31. Frisch, MJ., et al. Gaussian 09. Gaussian; Wallingford, CT: 2010. revision B.01
32. Morris GM, et al. Autodock4 and AutoDockTools4: automated docking with selective receptor flexibility. J Comput Chem. 2009; 16:2785–91. [PubMed: 19399780]
33. Liu H, Kornobis K, Lodowski P, Jaworska M, Kozlowski PM. TD-DFT insight into photodissociation of the Co-C bond in coenzyme B12. Front Chem. 2013; 1:1–12. [PubMed: 24790931]

Europe PMC Funders Author Manuscripts

Europe PMC Funders Author Manuscripts

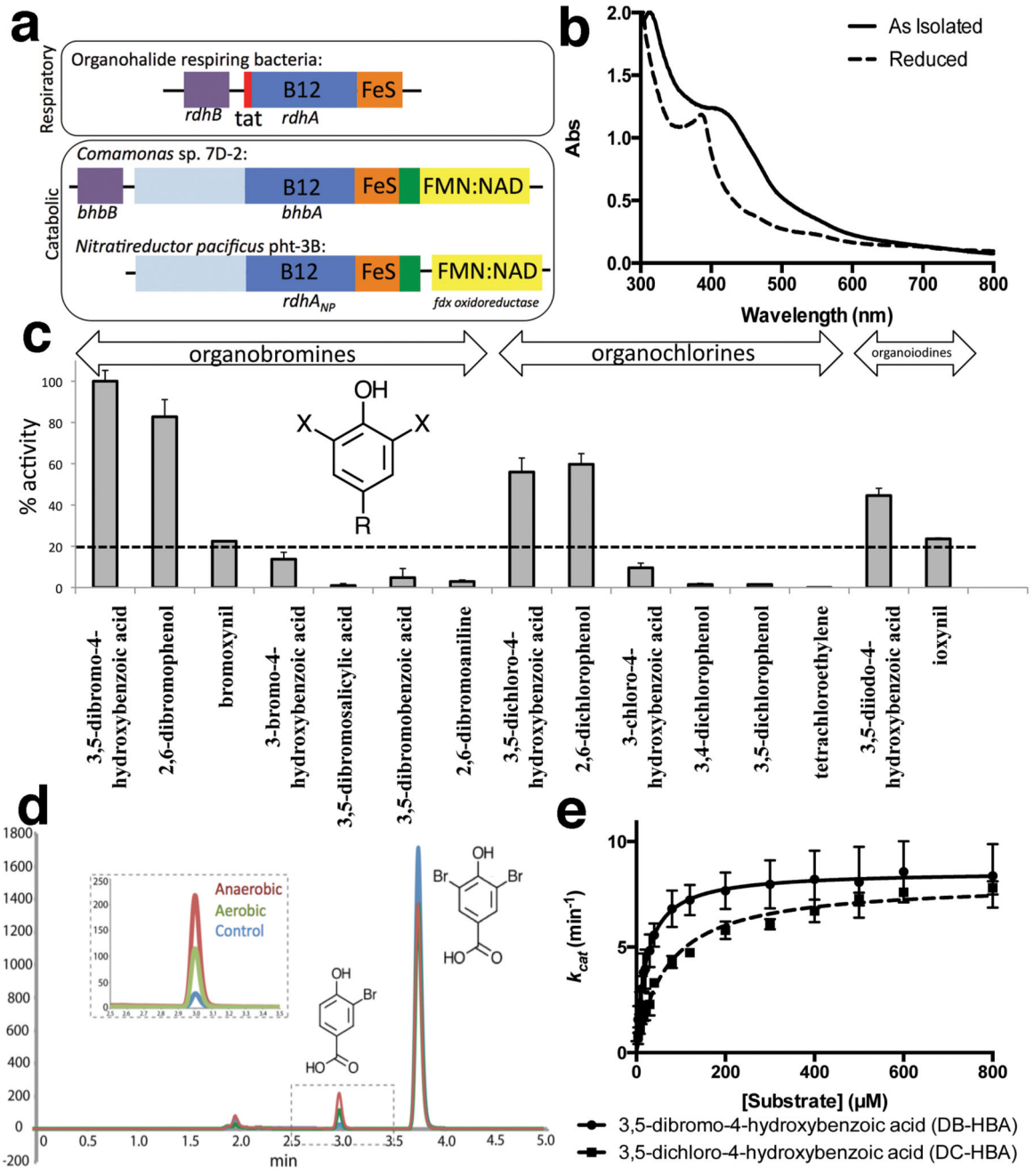

Fig. 1. Characterisation of RdhA$_{NP}$ as an *ortho*-dibromophenol reductase.

(a) Cartoon representation of the domain structure of the two reductive dehalogenase enzyme classes. **(b)** UV-Vis spectrum of 79 μM RdhA$_{NP}$ as purified under aerobic conditions and following reduction using deazaflavin and EDTA. The Co(I) concentration estimated using ε=26 000 M^{-1} cm^{-1} suggest 0.8 Co per RdhA$_{NP}$. **(c)** Relative activity with organohalide substrates using methyl viologen as electron donor. Results are shown as mean ± s.e.m; n=2. Highest activities (above the dotted line) were obtained when substrates resembled the 2,6-dihalophenol structure shown as inset. **(d)** HPLC product profiles

obtained when using spinach ferredoxin:$NADP^+$ oxidoreductase and ferredoxin to couple NADPH oxidation to $RdhA_{NP}$ 3,5-dibromo-4-hydroxybenzoic acid reductase activity. **(e)** Steady state kinetic profile obtained with 3,5-dibromo-4-hydroxybenzoic acid or 3,5-dichloro-4-hydroxybenzoic acid and reduced methyl viologen as substrates. Data points are shown as mean ± s.d; n=4.

Europe PMC Funders Author Manuscripts

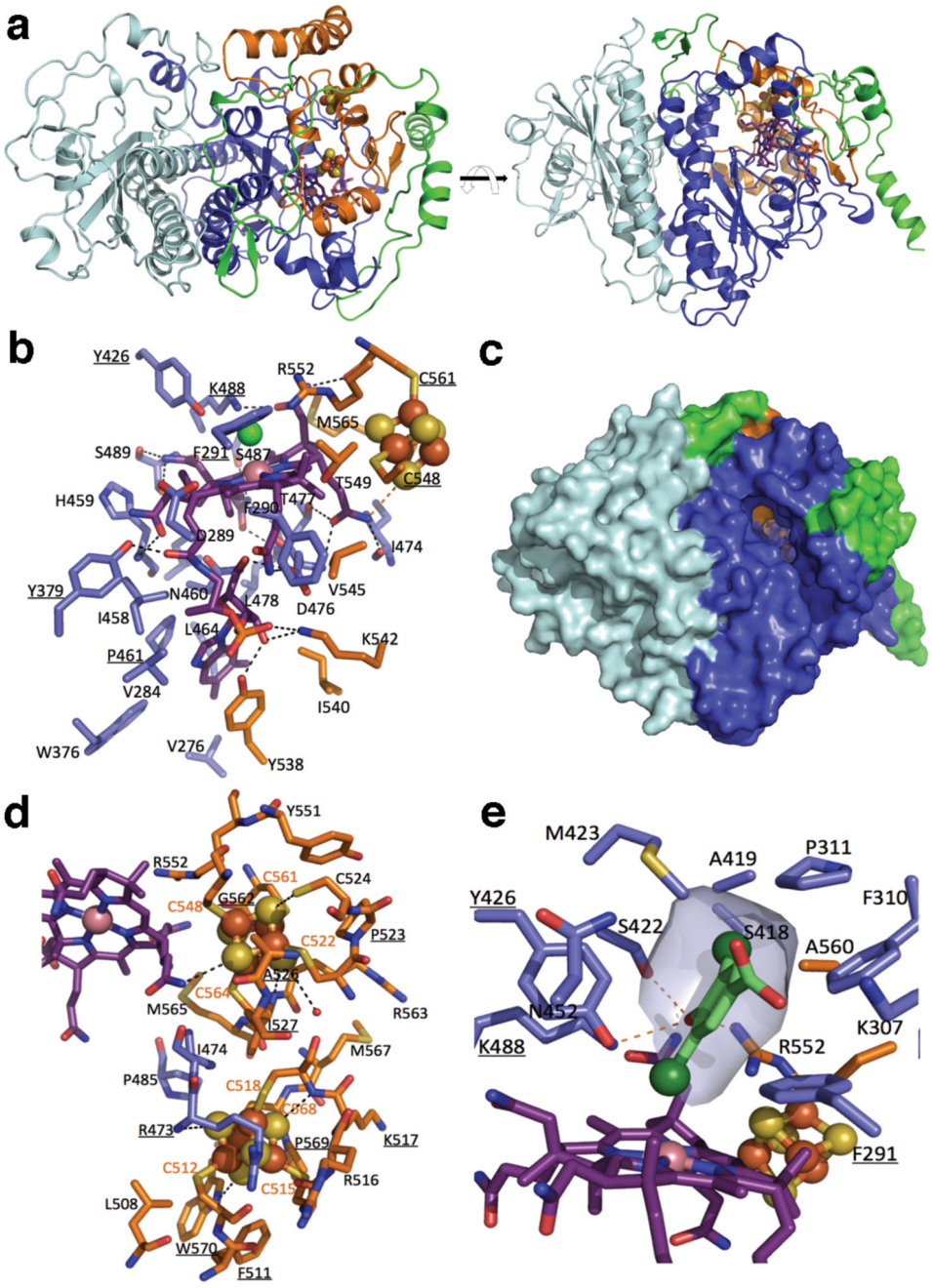

Fig. 2. Crystal structure of RdhA$_{NP}$ in the resting state.

(a) Overall structure of RdhA$_{NP}$ color coded according to domain structure as in Fig 1a and presented in two orientations. **(b)** Detailed view of the cobalamin binding pocket. Key residues are shown with carbons colored as in panel A. Direct polar interactions between cobalamin and the enzyme are indicated by black dashed lines. Residues that are conserved in an alignment of functionally characterized RdhAs are underlined. **(c)** Solvent accessible surface of RdhA$_{NP}$ color coded as in panel A, the orientation is similar to that of right hand panel 1a. **(d)** Detailed view of the 2x[4Fe-4S] cluster binding region, representation as in

panel B. **(e)** Detailed view of the RdhANP active site with a docked 3,5-dibromo-4-hydroxybenzoic acid substrate. Representation as in panel B, a transparent surface indicates the hydrophobic cavity that serves to bind the non-cobalt ligating bromine.

Europe PMC Funders Author Manuscripts

Europe PMC Funders Author Manuscripts

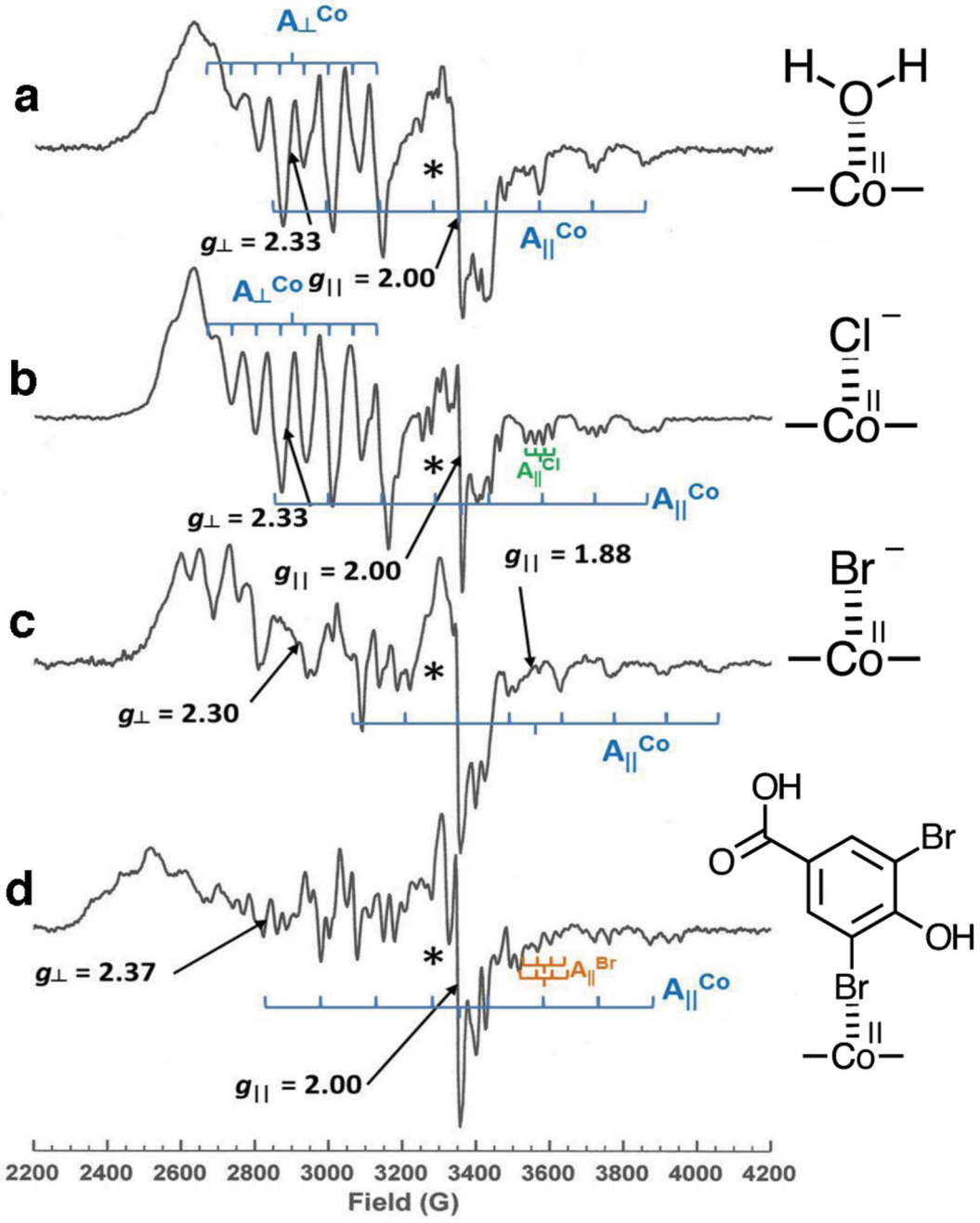

Fig. 3. EPR spectroscopy of RdhA$_{NP}$ reveals a direct halogen-cobalamin interaction.

X-band (~9.39 GHz) continuous wave (CW) of (**a**) 150 μM RdhA$_{NP}$ in non-halide containing buffer with *g* values marked. (**b**) RdhA$_{NP}$ plus 200 mM NaCl, with a 'quartet' arising from chloride (^{35}Cl) superhyperfine coupling indicated and g values marked (**c**) RdhA$_{NP}$ plus 25 mM KBr with *g* values marked. (**d**) RdhA$_{NP}$ plus 20 mM 3,5-dibromo-4-hydroxybenzoic acid with an example of the overlapped quartets arising from superhyperfine coupling to ^{79}Br and ^{81}Br indicated and *g* values marked. Key: Cobalt hyperfine coupling is indicated in blue (showing the eight expected for an I = 7/2 ^{59}Co),

halogen superhyperfine coupling (where present) is also indicated. For spectra C and D that exhibit overlapped $A_{\perp}^{Co}$ and $A_{\perp}^{Br}$ only $A_{||}^{Co}$ is indicated. For spectrum parameters, see Extended data Table 3. * indicates a superposition of a $[3Fe\text{-}4S]^{+}$ spectrum, the spectrum of a cob(III)alamin-superoxide species and an unassigned organic radical signal which together comprise less than 5% of the cob(II)alamin spectrum (see Extended data Fig. 4).

Europe PMC Funders Author Manuscripts

Europe PMC Funders Author Manuscripts

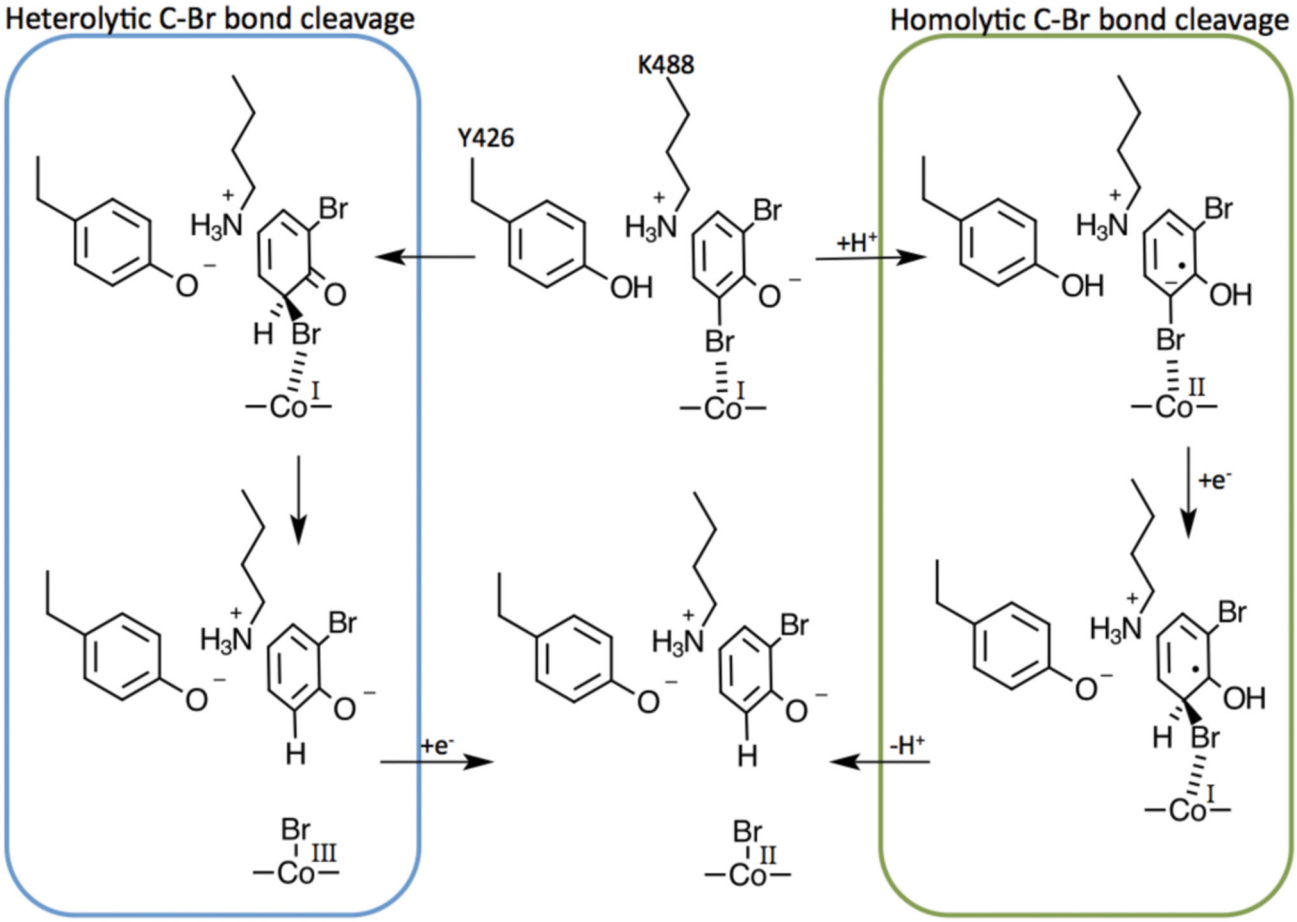

Fig. 4. $RdhA_{NP}$ proposed mechanism.

Our data suggest that the $RdhA_{NP}$ mechanism involves formation of a bromide-Cob(II)alamin complex either via heterolytic cleavage of the carbon-bromide substrate bond (in blue box) or homolytic cleavage of the carbon-bromide substrate bond (in green box). For clarity, only the 2,6-dibromophenol moiety of the substrate is shown.